Matched asymptotic expansions for bent and twisted rods: applications for cable and pipeline laying

D. M. STUMP and G. H. M. VAN DER HEIJDEN
Department of Mathematics, The University of Queensland, St. Lucia QLD 4072, Australia.
e-mail: dms@maths.uq.z.an

Abstract. The geometrically exact theory of linear elastic rods is used to formulate the general three-dimensional problem of a twisted, clamped rod hanging under gravity and subject to buoyancy forces from a fluid. The resulting boundary-value problem is solved by the method of matched asymptotic expansions. The truncated analytical solution is compared with results obtained from a numerical scheme and shows good agreement. The method is used to consider the near-catenary application of a clamped pipeline.

Key words: rod theory, matched asymptotic expansions, boundary layers, catenary, heavy cables, pipelines, buoyancy forces

1. Introduction

The problem of a long, twisted rod hanging under gravity occurs in a variety of industrial applications, such as pipeline laying, cable systems, and conveying. This paper considers a rod of arbitrary sag which is subject to clamped boundary conditions at the two ends and has also had twist inserted between the two ends. The objective is to develop a mathematical model for the three-dimensional stiffened catenary (including both gravity and buoyancy forces) and to solve the equations by means of matched asymptotics as well as numerical techniques.

In order to motivate a specific application, we idealise a pipeline being laid by the so-called 'J-lay' method from a barge on to the sea floor a distance D below, as shown in Figure 1. The pipeline is held clamped on deck of the vessel at an adjustable but fixed angle θ_1, with the sea surface, and approximately assumes the shape of a catenary. However, under the action of the wind the barge can undergo a displacement and yaw, which causes the cable to adopt a non-planar shape. This effect is included in the analysis in a quasi-static way through the prescription of the surface position and the angle ψ_1.

It is important to note at the outset that the example shown in Figure 1 is illustrative and is intended to place this work in an industrial setting. It is not our intention to provide a comprehensive model of all the practical issues, such as the 'S-lay' configuration or the use of stingers associated with pipeline laying and other industrial technologies. This is a detailed subject, and a more complete discussion of some of the difficulties associated with pipeline laying can be found in Brown and Elliott [1].

The problem of a clamped hanging rod has an extensive history in the applied mechanics literature. The shallow-sag problem is a prototype example in solid mechanics of the method of matched asymptotic expansions for linear equations (*e.g.* Nayfeh [2, pp. 387–415], Kevorkian and Cole [3, pp. 37–117]. The deeply sagged problem and the presence of
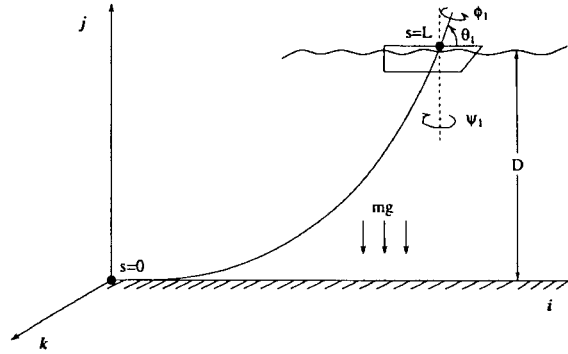
Figure 1. A pipeline being laid from a barge.

twist insertion complicates the analytical formulation and produces nonlinear boundary-layer equations. Despite the obvious importance, the problem of the deeply sagged rod hanging under gravity has a much more limited history of study.

Several papers in the literature deal with boundary layers in planar deep, stiffened catenaries. Plunkett [4] has attempted a matched asymptotic expansion for planar problems involving drill strings and hanging cables without twist. However, as Rienstra [5, pp. 99–108] has pointed out, in the formulation of the boundary-layer problem Plunkett linearises his Equation 14, which produces an inner-layer solution that is good only for small angular deflections from the horizontal, while the outer layer has large angular deflections. Consequently, the matching procedure is inaccurate. Dixon and Rutledge [6] perform the same analysis for the pipelaying problem and propagate this mistake. Konuk [7] attempts to correct the two-dimensional work in Plunkett [4], but continues to make the inner-layer solution mistake. Wolfe ([8] and [9]), uses the full three-dimensional Cosserat theory of rods to formulate the planar problem for a wide class of constitutive laws. He proves the existence of solutions, but does not obtain explicit solutions for any boundary-value problem.

There have also been numerical studies of the three-dimensional problem within the industrial context. Konuk [7] and [10], studies the three-dimensional pipelaying problem numerically, but considers only dead-load boundary conditions (*i.e.* prescribed end torque). The shortcomings of this approach have been pointed out by Brown and Elliot [1] who also treat the more realistic case of rigid boundary conditions (*i.e.* prescribed end rotation).

This study is an extension of work by Stump and Fraser [11] on the planar convection of fabric strips under gravity and low tension to the three-dimensional hanging cable. This paper makes two contributions: first, it gives the general formulation of the three-dimensional problem including twist, buoyancy, and general *clamped* boundary conditions; second, the leading-order nonlinear boundary-layer equation is solved exactly and matched to the outer solution for arbitrarily large deflections from the horizontal. The analytical expressions are compared with the results of numerical calculations and show good agreement.

This study is organised as follows. In Section 2, the mathematical formulation is developed and the key singular perturbation parameter is identified. In Section 3, the asymptotic analysis for both the inner and outer layers is developed and then matched by use of the notion of an intermediate length scale. In Section 4, the asymptotic results are compared to a sample of numerical calculations obtained from a stiff-equation solver. Section 5 closes the study with some final remarks.

2. Mathematical formulation

The large deflection theory of linear elastic rods is used to model the general problem of a rod hanging under gravity and in the presence of buoyancy forces from a surrounding fluid. The rod is assumed to be circular in cross-section, to be inextensible and unshearable, and to have a straight untwisted stress-free reference state.

The arclength parameter s for a rod of length L is measured from one end of the rod, and the vector function $\boldsymbol{R}(s)$, with components (X, Y, Z), describes the position of the centre line of the rod relative to a Cartesian co-ordinate frame $\{\boldsymbol{i}, \boldsymbol{j}, \boldsymbol{k}\}$ chosen such that the gravitational acceleration points in the $-\boldsymbol{j}$ direction.

2.1. THE GOVERNING EQUATIONS

The development of the equations governing the inextensible, flexible rod can be found in a number of references (*e.g.* Love [12, pp. 381–396]; Antman [13, pp. 259–323]; Champneys, van der Heijden, and Thompson [14]). The system of equations is:

$$
\begin{aligned}
& \left(T \boldsymbol{R}'\right)' + \boldsymbol{V}' - mg\,\boldsymbol{j} + \boldsymbol{F} = \boldsymbol{0}, \\
& \left(Q \boldsymbol{R}'\right)' + \boldsymbol{M}' + \boldsymbol{R}' \times \boldsymbol{V} = \boldsymbol{0}, \\
& \boldsymbol{R}' \cdot \boldsymbol{R}' = 1, \\
& \boldsymbol{R}' \cdot \boldsymbol{V} = 0, \\
& \boldsymbol{M} = B\left(\boldsymbol{R}' \times \boldsymbol{R}''\right), \\
& Q = K N',
\end{aligned}
\tag{1}
$$

where ( )′ denotes differentiation with respect to arclength s. The various physical quantities within Equation (1) are: the tension T; the shear force $\boldsymbol{V}$; the weight per arclength of the rod mg (m is mass per arclength and g is the gravitational acceleration); the buoyancy force per arclength $\boldsymbol{F}$; the twisting moment Q; the bending moment $\boldsymbol{M}$; the bending stiffness $B = EI$; the torsional stiffness $K = GJ$; and the rate of material twist N'. The constants G and E are, respectively, the shear modulus and Young's modulus. I is the second moment of area and J is the polar moment of inertia. For a circular cross-section rod it is straightforward to show that B and K are related by

$$
\frac{K}{B} = \frac{1}{1 + \nu},
\tag{2}
$$

where ν is Poisson's ratio.

The buoyancy force, which acts perpendicular to the tangent of the rod, has been considered for the planar rod by Pedersen [15], and is adapted for the three-dimensional rod in Appendix A. The buoyancy force is given by:

$$
\boldsymbol{F} = m_f g[\boldsymbol{j} - (\boldsymbol{R}' \cdot \boldsymbol{j})\boldsymbol{R}' + (D - \boldsymbol{R} \cdot \boldsymbol{j})\boldsymbol{R}''],
\tag{3}
$$

where m_f is the mass of the displaced fluid per arclength of the rod. For a cable hanging in air, m_f is often negligible in comparison to m, the mass density of the rod. However, for the pipeline application shown in Figure 1, m_f can be close to m.

It is worth pointing out that, despite the appearance, Equation (1) consists of only 11 independent equations due to the inextensibility constraint Equation $(1)_3$ which implies that all derivatives of $\boldsymbol{R}$ have only two independent components.

The integration of Equation (1) requires the specification of the 10 geometric boundary conditions

$$
\begin{aligned}
\boldsymbol{R}(0) &= \boldsymbol{A}_0, \quad \boldsymbol{R}'(0) = \boldsymbol{B}_0, \\
\boldsymbol{R}(L) &= \boldsymbol{A}_1, \quad \boldsymbol{R}'(L) = \boldsymbol{B}_1,
\end{aligned}
\tag{4}
$$

($\boldsymbol{B}_0$ and $\boldsymbol{B}_1$ are unit vectors and thus have only two independent components) and an additional equation involving the twisting moment Q. In order to find this last condition, first note that the formation of the scalar product of $\boldsymbol{R}'$ with Equation $(1)_2$ gives $Q' = 0$, which implies that Q is an unknown constant along the rod. There are two possibilities for specifying the final boundary condition:

1. *Specified torque.* The value of the constant Q is prescribed. This is a dead load situation.
2. *Specified rotation.* The values of all three Euler angles (θ, ψ, ϕ) shown in Figure 1 are prescribed. In order for this to be consistent with a constant twisting moment Q along the rod, it is necessary to keep track of the rotation of the rod about its axis along the length of the rod. In Appendix B an Euler angle formulation is used to derive the boundary condition

$$
\phi_1 = 2\pi Tw - \int_0^L \frac{\boldsymbol{R}' \cdot \boldsymbol{j}}{1 - (\boldsymbol{R}' \cdot \boldsymbol{j})^2} \left(\boldsymbol{R}' \times \boldsymbol{R}'' \right) \cdot \boldsymbol{j} \, ds,
\tag{5}
$$

where $Tw = N'L/(2\pi)$ is the total twist, and the Euler angle ϕ_1 describes the rotation of the rod about the tangent in the top-end clamp. As explained in Appendix B, under normal conditions we have $\phi_1 = 0$.

Thus, for rigid loading, ϕ_1 is imposed, $Q = 2\pi K Tw/L$ is unknown, and Equation (1) has to be solved in conjunction with Equation (5). For this, an iterative scheme may be used in which the total twist Tw is first guessed and successively updated by use of Equation (5).

The *clamped* boundary conditions presented in Equation (4) represent a fixed-grip situation where the vectors $\boldsymbol{R}''$ at the ends $s = 0$ and $s = L$ are computed as part of the solution process. In the pipe-laying process shown in Figure 1, the components of the tangent vector $\boldsymbol{B}_0$ and the total rod length L are not known *a priori* and must be found as part of the solution process by asserting that the components of the vector $\boldsymbol{R}''(0)$ vanish. Alternatively, the procedure presented below can be used to formulate a simply-supported boundary condition for $\boldsymbol{R}''(0)$ at the sea floor with the rod length L being determined by a lift-off condition, such as the vanishing of the vertical component of the tangent. However, since simply-supported boundary conditions generate rapid changes in the vector $\boldsymbol{R}''$, while clamped boundary conditions generate rapid changes in the *tangent* vector $\boldsymbol{R}'$, the former do not have as much effect on the position vector $\boldsymbol{R}$ as the latter due to the higher order of differentiation. Therefore, we confine our interest in this study to clamped boundary layers, which are more severe and potentially more likely to cause crimping.

To proceed with the analysis, dimensionless quantities (denoted by overbars) are formulated by reference to the length of the rod, L, and the weight of the buoyant rod, $m(1-\sigma)gL$, as the characteristic length and force, where the parameter

$$\sigma = \frac{m_f}{m}$$

is the ratio of the fluid to rod densities (the inverse of the specific gravity). The resulting dimensionless quantities are given by

$$\bar{s} = \frac{s}{L}, \quad \bar{F} = \frac{F}{m(1-\sigma)g}, \quad \kappa = \frac{K}{B}, \quad \bar{R} = \frac{R}{L},$$

$$\bar{M} = \frac{M}{m(1-\sigma)gL^2}, \quad \bar{Q} = \frac{Q}{m(1-\sigma)gL^2}, \quad \bar{N}' = LN', \quad (6)$$

$$\bar{T} = \frac{T}{m(1-\sigma)gL}, \quad \bar{V} = \frac{V}{m(1-\sigma)gL}, \quad \bar{D} = \frac{D}{L}.$$

These are substituted in Equation (1) to provide the dimensionless system (*overbars are dropped hereafter*)

$$\left(T\boldsymbol{R}'\right)' + \boldsymbol{V}' - \boldsymbol{j}/(1-\sigma) + \boldsymbol{F} = \boldsymbol{0},$$

$$\left(Q\boldsymbol{R}'\right)' + \boldsymbol{M}' + \boldsymbol{R}' \times \boldsymbol{V} = \boldsymbol{0},$$

$$\boldsymbol{R}' \cdot \boldsymbol{R}' = 1,$$

$$\boldsymbol{R}' \cdot \boldsymbol{V} = 0, \quad (7)$$

$$\boldsymbol{M} = \varepsilon^2 \left(\boldsymbol{R}' \times \boldsymbol{R}''\right),$$

$$Q = \kappa \varepsilon^2 N',$$

where the dimensionless bending rigidity parameter

$$\varepsilon^2 = \frac{B}{m(1-\sigma)gL^3}$$

is typically $<< O(1)$. The dimensionless buoyancy force Equation (3) has the form

$$\boldsymbol{F} = \frac{\sigma}{1-\sigma}[\boldsymbol{j} - (\boldsymbol{R}' \cdot \boldsymbol{j})\boldsymbol{R}' + (D - \boldsymbol{R} \cdot \boldsymbol{j})\boldsymbol{R}'']. \quad (8)$$

The dimensionless forms of the geometric boundary conditions are still given by Equation (4) (except the L is replaced with 1), while the final twist boundary condition is given either by

$$Q = \varepsilon^2(2\pi\kappa Tw), \quad (9)$$

or by Equation (5). In many applications, Tw is $O(1)$, so Q is $O(\varepsilon^2)$, which is assumed to be the case in the remainder of this study. This completes the formulation of the governing equations.

2.2. INTEGRATION OF THE EQUATIONS

The integration of the governing equations is accomplished as follows. First, Equation (8) is substituted in $(7)_1$, and the result is then integrated to obtain

$$\left(T + \frac{\sigma D}{1 - \sigma}\right) \mathbf{R}' + \mathbf{V} - s\mathbf{j} - \frac{\sigma(\mathbf{R} \cdot \mathbf{j})\mathbf{R}'}{1 - \sigma} + \mathbf{C} = \mathbf{0}, \tag{10}$$

where $\mathbf{C}$ is a constant vector to be determined as part of the problem. Next, the formation of the vector product of $\mathbf{R}'$ with Equation $(7)_2$ and the elimination of Q and M via Equations (9) and $(7)_5$ gives

$$\mathbf{V} = \varepsilon^2 \left\{ 2\pi\kappa T w (\mathbf{R}' \times \mathbf{R}'') - \mathbf{R}''' - \mathbf{R}'(\mathbf{R}'' \cdot \mathbf{R}'') \right\}, \tag{11}$$

where use has also been made of the relationship $\mathbf{R}' \cdot \mathbf{R}''' = -\mathbf{R}'' \cdot \mathbf{R}''$ obtained from the differentiation of Equation $(7)_3$. The formation of the scalar product of $\mathbf{R}'$ with Equation (10) yields an expression for the tension T,

$$T = s(\mathbf{R}' \cdot \mathbf{j}) - \mathbf{C} \cdot \mathbf{R}' + \frac{\sigma(\mathbf{R} \cdot \mathbf{j} - D)}{1 - \sigma}, \tag{12}$$

which is inserted with Equation (11) in Equation (10) to obtain

$$\begin{aligned}
&\left\{ s(\mathbf{R}' \cdot \mathbf{j}) - \mathbf{C} \cdot \mathbf{R}' \right\} \mathbf{R}' - s\mathbf{j} + \mathbf{C} \\
&+ \varepsilon^2 \left\{ 2\pi\kappa T w (\mathbf{R}' \times \mathbf{R}'') - \mathbf{R}''' - \mathbf{R}'(\mathbf{R}'' \cdot \mathbf{R}'') \right\} = \mathbf{0}.
\end{aligned} \tag{13}$$

This is an extraordinary equation for the shape of the rod, since the buoyancy parameter σ has dropped out explicitly; it does, of course, still figure in the nondimensionalisation and in the rod tension Equation (12). The next section discusses the asymptotic analysis needed to solve Equation (13).

3. Asymptotic analysis

The solution of Equation (13) follows the classical methods of singular perturbation theory Kevorkian and Cole [3, pp. 36–117]. Away from the ends of the rod (*i.e.* the *outer* region), the tension force T is an $O(1)$ quantity, while the other forces and moments are at most $O(\varepsilon)$. Near the clamped ends, the tangent vector *may* change rapidly, depending on the boundary conditions, over the scaled distance $\xi = s/\varepsilon$ so that T and $\mathbf{V}$ are $O(1)$, in which case there is a boundary layer in the *inner* region. The solution of Equation (13) in the inner and outer regions is considered separately, and the solutions are then patched together by matching with an intermediate co-ordinate.

3.1. THE OUTER SOLUTION

The quantities $\mathbf{R}(s)$ and $\mathbf{C}$ are expanded in regular perturbation series in the parameter ε:

$$\begin{aligned}
\mathbf{R}(s) &= \mathbf{R}_0(s) + \varepsilon \mathbf{R}_1(s) + \varepsilon^2 \mathbf{R}_2(s) + \cdots, \\
\mathbf{C} &= \mathbf{C}_0 + \varepsilon \mathbf{C}_1 + \varepsilon^2 \mathbf{C}_2 + \cdots,
\end{aligned} \tag{14}$$

which are substituted in Equation (13) to obtain a succession of equations in powers of ε, the first two of which are

$$O(1): \quad \left\{ s(\boldsymbol{R}_0' \cdot \boldsymbol{j}) - \boldsymbol{C}_0 \cdot \boldsymbol{R}_0' \right\} \boldsymbol{R}_0' - s\boldsymbol{j} + \boldsymbol{C}_0 = \boldsymbol{0},$$

$$O(\varepsilon): \quad s(\boldsymbol{R}_0' \cdot \boldsymbol{j})\boldsymbol{R}_1' + s(\boldsymbol{R}_1' \cdot \boldsymbol{j})\boldsymbol{R}_0' - (\boldsymbol{C}_1 \cdot \boldsymbol{R}_0')\boldsymbol{R}_0' \tag{15}$$
$$- (\boldsymbol{C}_0 \cdot \boldsymbol{R}_1')\boldsymbol{R}_0' - (\boldsymbol{C}_0 \cdot \boldsymbol{R}_0')\boldsymbol{R}_1' + \boldsymbol{C}_1 = \boldsymbol{0}.$$

The use of the inextensibility condition Equation $(7)_3$ provides the additional constraints that $\boldsymbol{R}_0' \cdot \boldsymbol{R}_0' = 1$ and $\boldsymbol{R}_0' \cdot \boldsymbol{R}_1' = 0$.

The $O(1)$ solution is obtained as follows. The expressions $\boldsymbol{R}_0 = x_0\boldsymbol{i} + y_0\boldsymbol{j} + z_0\boldsymbol{k}$ and $\boldsymbol{C}_0 = c_x\boldsymbol{i} + c_y\boldsymbol{j} + c_z\boldsymbol{k}$ are inserted into Equation $(15)_1$ in order to produce a set of component equations that are solved by elementary means. The $O(1)$ solution is

$$x_0 = -|c_x|\sinh^{-1}\left\{ \frac{c_y - s}{\sqrt{c_x^2 + c_z^2}} \right\} + |c_x|\sinh^{-1}\left\{ \frac{c_y}{\sqrt{c_x^2 + c_z^2}} \right\} + X_0,$$

$$y_0 = -\alpha\sqrt{c_x^2 + (c_y - s)^2 + c_z^2} + \alpha\sqrt{c_x^2 + c_y^2 + c_z^2} + Y_0, \tag{16}$$

$$z_0 = \frac{c_z}{c_x}x_0 + Z_0,$$

where $\alpha = c_x/|c_x|$, and (X_0, Y_0, Z_0) are additional constants of integration. This is the three-dimensional catenary lying in a plane making an angle $\chi = \arctan(c_z/c_x)$ with the $(\boldsymbol{i}, \boldsymbol{j})$ co-ordinate plane. The constants (c_x, c_y, c_z) are still unknown and will be determined in the matching process. We can already observe, however, that solutions come in pairs (concave-up or concave-down) as the x_0 and z_0 components of Equation (16) are invariant under a simultaneous sign change of c_x and c_z.

The solution to the $O(\varepsilon)$ equation is found from the formation of two successive vector products of $\boldsymbol{R}_0'$ with Equation $(15)_2$, which yields:

$$\boldsymbol{R}_0' \times (\boldsymbol{R}_0' \times \boldsymbol{R}_1') \left\{ s(\boldsymbol{R}_0' \cdot \boldsymbol{j}) - \boldsymbol{C}_0 \cdot \boldsymbol{R}_0' \right\} + \boldsymbol{R}_0' \times (\boldsymbol{R}_0' \times \boldsymbol{C}_1) = \boldsymbol{0}. \tag{17}$$

The use of the triple vector product identity and inextensibility gives

$$\boldsymbol{R}_1' = \frac{\boldsymbol{R}_0'(\boldsymbol{R}_0' \cdot \boldsymbol{C}_1) - \boldsymbol{C}_1}{s(\boldsymbol{R}_0' \cdot \boldsymbol{j}) - \boldsymbol{C}_0 \cdot \boldsymbol{R}_0'}. \tag{18}$$

The solution of Equation (18) for $\boldsymbol{R}_1 = x_1\boldsymbol{i} + y_1\boldsymbol{j} + z_1\boldsymbol{k}$ and $\boldsymbol{C}_1 = d_x\boldsymbol{i} + d_y\boldsymbol{j} + d_z\boldsymbol{k}$ is obtained through the use of Equation (16) along with elementary integrations to yield

$$\begin{aligned}
\boldsymbol{R}_1(s) = &\left\{ (-|c_x|c_z d_z + \alpha c_z^2 d_x)I_1(s) - |c_x|d_y\, I_2(s) + \alpha d_x\, I_3(s) \right\} \boldsymbol{i} \\
&+ \left\{ \alpha(c_x^2 d_y + c_z^2 d_y)I_1(s) - (\alpha c_z d_z + |c_x|d_x)I_2(s) \right\} \boldsymbol{j} \\
&+ \left\{ (-|c_x|c_z d_x + \alpha c_x^2 d_z)I_1(s) - \alpha c_z d_y\, I_2(s) + \alpha d_z\, I_3(s) \right\} \boldsymbol{k} \\
&+ X_1\boldsymbol{i} + Y_1\boldsymbol{j} + Z_1\boldsymbol{k},
\end{aligned} \tag{19}$$

where (X_1, Y_1, Z_1) are integration constants and

$$I_1(s) = -\frac{c_y - s}{(c_x^2 + c_z^2)\sqrt{c_x^2 + (c_y - s)^2 + c_z^2}},$$

$$I_2(s) = \frac{1}{\sqrt{c_x^2 + (c_y - s)^2 + c_z^2}},$$

$$I_3(s) = \frac{c_y - s}{\sqrt{c_x^2 + (c_y - s)^2 + c_z^2}} - \sinh^{-1}\left(\frac{c_y - s}{\sqrt{c_x^2 + c_z^2}}\right).$$

3.2. THE INNER SOLUTION

The solution to Equation (13) may have boundary layers at either end. We derive the form of the boundary layer solution near $s = 0$ and subsequently adapt this result to obtain the solution near $s = 1$.

Within the boundary layer near $s = 0$ the tangent vector changes rapidly on $O(s/\varepsilon)$, so we introduce the scaled co-ordinate $\xi = s/\varepsilon$ and expand the position vector with the series

$$\boldsymbol{R}(s) = \boldsymbol{A}_0 + \varepsilon\hat{\boldsymbol{R}}(\xi) = \boldsymbol{A}_0 + \varepsilon\hat{\boldsymbol{R}}_0(\xi) + \varepsilon^2\hat{\boldsymbol{R}}_1(\xi) + \cdots . \tag{20}$$

In the boundary layer, Equation (13) is rewritten in terms of $\hat{\boldsymbol{R}}(\xi)$ as

$$\left\{\varepsilon\xi(\hat{\boldsymbol{R}}' \cdot \boldsymbol{j}) - \boldsymbol{C} \cdot \hat{\boldsymbol{R}}'\right\}\hat{\boldsymbol{R}}' - \hat{\boldsymbol{R}}''' - \hat{\boldsymbol{R}}'(\hat{\boldsymbol{R}}'' \cdot \hat{\boldsymbol{R}}'')$$

$$+ \varepsilon 2\pi\kappa T w(\hat{\boldsymbol{R}}' \times \hat{\boldsymbol{R}}'') - \varepsilon\xi\boldsymbol{j} + \boldsymbol{C} = \boldsymbol{0}, \tag{21}$$

where $\hat{\boldsymbol{R}}' = \mathrm{d}\hat{\boldsymbol{R}}/\mathrm{d}\xi$. The insertion of Equations (14)$_2$ and (20) in Equation (21) provides a hierarchy of equations in powers of ε, the first two of which are

$$O(1): \quad (\boldsymbol{C}_0 \cdot \hat{\boldsymbol{R}}_0')\hat{\boldsymbol{R}}_0' + \hat{\boldsymbol{R}}_0''' + \hat{\boldsymbol{R}}_0'(\hat{\boldsymbol{R}}_0'' \cdot \hat{\boldsymbol{R}}_0'') = \boldsymbol{C}_0,$$

$$O(\varepsilon): \quad \xi(\hat{\boldsymbol{R}}_0' \cdot \boldsymbol{j})\hat{\boldsymbol{R}}_0' - (\boldsymbol{C}_1 \cdot \hat{\boldsymbol{R}}_0')\hat{\boldsymbol{R}}_0' - (\boldsymbol{C}_0 \cdot \hat{\boldsymbol{R}}_1')\hat{\boldsymbol{R}}_0'$$

$$- (\boldsymbol{C}_0 \cdot \hat{\boldsymbol{R}}_0')\hat{\boldsymbol{R}}_1' - \hat{\boldsymbol{R}}_1''' - \hat{\boldsymbol{R}}_1'(\hat{\boldsymbol{R}}_0'' \cdot \hat{\boldsymbol{R}}_0'') - 2\hat{\boldsymbol{R}}_0'(\hat{\boldsymbol{R}}_1'' \cdot \hat{\boldsymbol{R}}_0'') \tag{22}$$

$$- \xi\boldsymbol{j} + 2\pi\kappa T w(\hat{\boldsymbol{R}}_0' \times \hat{\boldsymbol{R}}_0'') + \boldsymbol{C}_1 = \boldsymbol{0}.$$

It is noted that for $O(1)$ values of Tw, twist appears first in the $O(\varepsilon)$ equation.

The solution to the $O(1)$ equation is obtained by forming the vector product of $\hat{\boldsymbol{R}}_0'$ with Equation (22)$_1$ to get

$$(\hat{\boldsymbol{R}}_0' \times \hat{\boldsymbol{R}}_0'')' = (\hat{\boldsymbol{R}}_0 \times \boldsymbol{C}_0)', \tag{23}$$

and then integrating this, we have

$$\hat{\boldsymbol{R}}_0' \times \hat{\boldsymbol{R}}_0'' = \hat{\boldsymbol{R}}_0 \times \boldsymbol{C}_0 + \boldsymbol{D}_0, \tag{24}$$

where $\boldsymbol{D}_0$ is a constant integration vector. Equation (24) is the equation for the planar elastica whose solution has been considered by Coyne [16].

In accordance with the principle of least degeneracy (Van Dyke [17, pp. 86–87]), it is expected that as $\xi \to \infty$, $\hat{\boldsymbol{R}}_0$ decays asymptotically to a straight line with the form $\hat{\boldsymbol{R}}_0 \sim \xi \hat{\boldsymbol{R}}_0'(\infty)$, where $\hat{\boldsymbol{R}}_0'(\infty)$ is a still undetermined constant vector. In order to find $\hat{\boldsymbol{R}}_0'(\infty)$, we take the limit of Equation (24) as $\xi \to \infty$, which requires that $\hat{\boldsymbol{R}}_0'(\infty) = \boldsymbol{C}_0$ in order for the right side of Equation (24) to remain bounded. Also note that the tangent vector $\hat{\boldsymbol{R}}_0'$ in the boundary layer starts out equal to $\boldsymbol{B}_0$ at $\xi = 0$. Thus, we expect the inner solution $\hat{\boldsymbol{R}}_0$ to lie in the plane spanned by $\boldsymbol{B}_0$ and $\boldsymbol{C}_0$ since twist has no effect at this order of approximation. It is convenient to define a set of basis vectors $(\boldsymbol{e}_\rho, \boldsymbol{e}_\eta, \boldsymbol{N})$ by

$$N = \alpha \frac{C_0}{|C_0|}, \qquad e_\eta = \frac{B_0 \times N}{|B_0 \times N|}, \qquad e_\rho = e_\eta \times N, \tag{25}$$

so that $\hat{\boldsymbol{R}}_0$ lies in the $(\boldsymbol{e}_\rho, \boldsymbol{N})$ plane. Thus, we expect the inner solution to have the form

$$\hat{\boldsymbol{R}}_0(\xi) = [\rho(\xi) - \rho_\infty]\boldsymbol{e}_\rho + h(\xi)\boldsymbol{N}, \tag{26}$$

where, as $\xi \to \infty$, the components $\rho(\xi)$ and $h(\xi)$ approach the values

$$\rho \to 0, \quad h \to \xi, \quad \rho' \to 0, \quad h' \to 1,$$

and ρ is restricted to the range $0 \leqslant \rho \leqslant \rho_\infty$. The introduction of Equation (26) into Equation (24) and the taking of the limit $\xi \to \infty$ gives

$$\boldsymbol{D}_0 = -\alpha \rho_\infty |\boldsymbol{C}_0| \boldsymbol{e}_\eta, \tag{27}$$

since $\hat{\boldsymbol{R}}_0'' \to \boldsymbol{0}$. Next, the elimination of $\boldsymbol{D}_0$ from Equation (24) and the formation of the vector product with $\hat{\boldsymbol{R}}_0'$ yields the equation

$$\hat{\boldsymbol{R}}_0'' = -\alpha \hat{\boldsymbol{R}}_0' \times \left[\hat{\boldsymbol{R}}_0 \times \boldsymbol{N} - \rho_\infty \boldsymbol{e}_\eta \right] |\boldsymbol{C}_0|, \tag{28}$$

which is further simplified with the introduction of the rescaled co-ordinate

$$r = \alpha |\boldsymbol{C}_0| \xi, \qquad \frac{\mathrm{d}}{\mathrm{d}\xi} = \alpha |\boldsymbol{C}_0| \frac{\mathrm{d}}{\mathrm{d}r}, \tag{29}$$

to obtain

$$\frac{\mathrm{d}^2 \hat{\boldsymbol{R}}_0}{\mathrm{d}r^2} = -\frac{\mathrm{d}\hat{\boldsymbol{R}}_0}{\mathrm{d}r} \times \left[\hat{\boldsymbol{R}}_0 \times \boldsymbol{N} - \rho_\infty \boldsymbol{e}_\eta \right]. \tag{30}$$

Equation (30) provides the separated component equations:

$$\frac{\mathrm{d}^2 \rho}{\mathrm{d}r^2} = -\rho \frac{\mathrm{d}h}{\mathrm{d}r}, \qquad \frac{\mathrm{d}^2 h}{\mathrm{d}r^2} = \rho \frac{\mathrm{d}\rho}{\mathrm{d}r}. \tag{31}$$

Straightforward integration and use of the boundary conditions as $r \to \infty$, along with the inextensibility constraint $|\mathrm{d}\hat{\boldsymbol{R}}_0/\mathrm{d}r| = |\boldsymbol{C}_0|$, gives

$$\frac{\mathrm{d}\rho}{\mathrm{d}r} = \alpha\rho\sqrt{\frac{1}{|\boldsymbol{C}_0|} - \frac{\rho^2}{4}}, \qquad \frac{\mathrm{d}h}{\mathrm{d}r} = \frac{\alpha}{|\boldsymbol{C}_0|} + \frac{\rho^2}{2}. \tag{32}$$

Further integration yields the solution

$$\rho = \frac{2}{\sqrt{|\boldsymbol{C}_0|}} \operatorname{sech}\left(\frac{\alpha r}{\sqrt{|\boldsymbol{C}_0|}} + r_0\right),$$

$$h = h_0 + \frac{\alpha r}{|\boldsymbol{C}_0|} - \frac{2}{\sqrt{|\boldsymbol{C}_0|}} \tanh\left(\frac{\alpha r}{\sqrt{|\boldsymbol{C}_0|}} + r_0\right), \tag{33}$$

where r_0 and h_0 are integration constants. The rescaled co-ordinate r is eliminated from these expressions, which are then substituted in Equation (26) to obtain the leading-order inner-layer solution

$$\hat{\boldsymbol{R}}_0(\xi) = \left[\frac{2}{\sqrt{|\boldsymbol{C}_0|}} \operatorname{sech}\left(\xi\sqrt{|\boldsymbol{C}_0|} + r_0\right) - \rho_\infty\right]\boldsymbol{e}_\rho$$

$$+ \left[h_0 + \xi - \frac{2}{\sqrt{|\boldsymbol{C}_0|}} \tanh\left(\xi\sqrt{|\boldsymbol{C}_0|} + r_0\right)\right]\boldsymbol{N}. \tag{34}$$

The integration constants (r_0, ρ_∞, h_0) are determined by the boundary conditions at $\xi = 0$, that is, $\hat{\boldsymbol{R}}_0(0) = \boldsymbol{0}$ and $\mathrm{d}\hat{\boldsymbol{R}}_0(0)/\mathrm{d}\xi = \boldsymbol{B}_0$, which give the formulas

$$r_0 = \operatorname{sech}^{-1}\left\{\left(\frac{1}{2} - \frac{1}{2}\sqrt{1 - \frac{|\boldsymbol{B}_0 \times \boldsymbol{C}_0|^2}{|\boldsymbol{C}_0|^2}}\right)^{1/2}\right\},$$

$$\rho_\infty = \frac{2}{\sqrt{|\boldsymbol{C}_0|}} \operatorname{sech} r_0, \qquad h_0 = \frac{2}{\sqrt{|\boldsymbol{C}_0|}} \tanh r_0. \tag{35}$$

In order to obtain a solution for the boundary layer near $s = 1$, we introduce the scaled co-ordinate $\zeta = (1 - s)/\varepsilon$ and the expansion

$$\boldsymbol{R}(s) = \boldsymbol{A}_1 + \varepsilon\check{\boldsymbol{R}}(\zeta) = \boldsymbol{A}_1 + \varepsilon\check{\boldsymbol{R}}_0(\zeta) + \varepsilon^2\check{\boldsymbol{R}}_1(\zeta) + \cdots. \tag{36}$$

An analysis similar to the one above gives

$$\check{\boldsymbol{R}}_0(\zeta) = \left[\frac{2}{\sqrt{|\boldsymbol{j} - \boldsymbol{C}_0|}} \operatorname{sech}\left(\zeta\sqrt{|\boldsymbol{j} - \boldsymbol{C}_0|} + r_1\right) - \sigma_\infty\right]\boldsymbol{e}_\sigma$$

$$+ \left[h_1 + \zeta - \frac{2}{\sqrt{|\boldsymbol{j} - \boldsymbol{C}_0|}} \tanh\left(\zeta\sqrt{|\boldsymbol{j} - \boldsymbol{C}_0|} + r_1\right)\right]\boldsymbol{P}, \tag{37}$$

where the local vector system near $s = 1$ is given by

$$\boldsymbol{P} = \alpha\frac{\boldsymbol{j} - \boldsymbol{C}_0}{|\boldsymbol{j} - \boldsymbol{C}_0|}, \qquad \boldsymbol{e}_\gamma = -\frac{\boldsymbol{B}_1 \times \boldsymbol{P}}{|\boldsymbol{B}_1 \times \boldsymbol{P}|}, \qquad \boldsymbol{e}_\sigma = \boldsymbol{e}_\gamma \times \boldsymbol{P}. \tag{38}$$

The integration constants $(r_1, \sigma_\infty, h_1)$ are determined by the boundary conditions at $\zeta = 0$, that is, $\check{R}_0(0) = \mathbf{0}$ and $\mathrm{d}\check{R}_0(0)/\mathrm{d}\zeta = -B_1$, which give the formulas

$$r_1 = \mathrm{sech}^{-1}\left\{\left(\frac{1}{2} - \frac{1}{2}\sqrt{1 - \frac{|B_1 \times (j - C_0)|^2}{|j - C_0|^2}}\right)^{1/2}\right\},$$

(39)

$$\sigma_\infty = \frac{2}{\sqrt{|j - C_0|}}\,\mathrm{sech}\,r_1, \qquad h_1 = \frac{2}{\sqrt{|j - C_0|}}\,\tanh r_1.$$

3.3. MATCHING THE INNER AND OUTER SOLUTIONS

The matching between the inner and outer solutions is conducted with the method of intermediate co-ordinates (Kevorkian and Cole [3, pp. 36–117]). At the left-hand boundary, the arclength s and the boundary-layer co-ordinate ξ are both expressed in terms of an intermediate co-ordinate $\eta(\varepsilon)$ by

$$s = \eta\tau, \qquad \xi = \frac{\eta\tau}{\varepsilon},$$

where $\eta(\varepsilon)$ is such that $\eta(\varepsilon)$ and $\varepsilon/\eta(\varepsilon)$ are both $o(1)$, and τ is fixed. The inner solution at $s = 0$ has the form:

$$R(s) = A_0 + \varepsilon\hat{R}_0\left(\frac{\eta\tau}{\varepsilon}\right) + \cdots,$$

(40)

while the outer expansion becomes

$$R(s) = R_0(\eta\tau) + \varepsilon R_1(\eta\tau) + \cdots.$$

(41)

The matching process

$$\lim_{\varepsilon\to 0}\left\{A_0 + \varepsilon\hat{R}_0\left(\frac{\eta\tau}{\varepsilon}\right) + \cdots\right\} = \lim_{\varepsilon\to 0}\{R_0(\eta\tau) + \varepsilon R_1(\eta\tau) + \cdots\}$$

(42)

leads to the $O(1)$ and $O(\varepsilon)$ conditions:

$$A_0 = R_0(0),$$
$$-\rho_\infty e_\rho + \left(h_0 - \frac{2}{\sqrt{|C_0|}}\right)N = R_1(0).$$

(43)

Note that the first equation determines the constants (X_0, Y_0, Z_0).

A similar matching process between the outer solution and the inner solution near $s = 1$ gives the $O(1)$ and $O(\varepsilon)$ equations:

$$A_1 = R_0(1),$$
$$-\sigma_\infty e_\sigma + \left(h_1 - \frac{2}{\sqrt{|j - C_0|}}\right)P = R_1(1).$$

(44)

Equation $(44)_1$ provides a set of three nonlinear equations for the determination of $\boldsymbol{C}_0$. There are two solutions: a tensile solution (concave up) with $c_x < 0$ and a compressive solution (concave down) with $c_x > 0$. Since typically the $c_x < 0$ solution is the physically realised one, only this solution is considered in the present study. Once $\boldsymbol{C}_0$ is known, $(r_0, h_0, \rho_\infty, r_1, h_1, \sigma_\infty)$ are found from Equations (35) and (39). Equations $(43)_2$ and $(44)_2$ then provide six linear equations for the components of $\boldsymbol{C}_1$ and the integration constants (X_1, Y_1, Z_1). Higher-order constant terms (*e.g.* $\boldsymbol{C}_2$ in the $\boldsymbol{C}$ expansion of Equation $(14)_2$) can be obtained by solving for additional terms in the inner and outer solutions and continuing with the matching process. This is a difficult task since the higher order inner-layer equations (*e.g.* Equation $(22)_2$) can no longer be solved analytically.

4. Comparison with numerical results

In this section we compare the truncated analytical solution constructed in the previous section with results obtained by numerically integrating Equation (13). We will only consider the case of specified rotation, in which Equation (5) is enforced. The boundary conditions at the water surface $s = 1$ are then naturally expressed in terms of Euler angles. The angles defined in the Appendix B are as follows: $\theta_1 := \theta(1)$ is the stern angle; $\psi_1 := \psi(1)$ the yaw angle of the ship; and $\phi_1 := \phi(1)$ the rotation angle of the rod in the clamp. With these definitions, $\boldsymbol{B}_1$ in Equation (4) can be written in terms of the Euler angles as

$$\boldsymbol{B}_1 = \cos\psi_1 \cos\theta_1 \boldsymbol{i} + \sin\theta_1 \boldsymbol{j} + \sin\psi_1 \cos\theta_1 \boldsymbol{k}. \tag{45}$$

For simplicity we take $\boldsymbol{A}_0 = \boldsymbol{0}$, $\boldsymbol{B}_0 = \boldsymbol{i}$. Solution of the problem then requires the specification of the following six parameters:

$$a_1, \quad a_2, \quad a_3, \quad \theta_1, \quad \psi_1, \quad \phi_1, \tag{46}$$

where (a_1, a_2, a_3) are the dimensionless components of $\boldsymbol{A}_1$.

The system is solved numerically by using COLNEW, a slightly modified version of the general-purpose collocation code COLSYS (Ascher *et al.* [18]) for solving boundary-value problems in ordinary differential equations. Once a solution to the problem is found, the bending moment and tension can be obtained from the Equations $(7)_5$ and (12), respectively, and the shear force, subsequently, from Equation (10). Although the system of equations is stiff for small ε, COLNEW experiences no problems with ε as small as 0·001, provided a sufficiently fine mesh is used. Convergence problems when integrating the stiff system of equations for a twisted pipeline have been reported by Konuk [10].

Figure 2 shows a comparison of the analytical results with the numerical calculations for $a_1 = 0.75, a_2 = 0.2$, $a_3 = 0.1$ and $\theta_1 = 0$, $\psi_1 = -\pi/2$ and $\phi_1 = 0$ for $\varepsilon = 0.05$. (From a mathematical viewpoint, this is not a particularly small value of ε and has been chosen so that the differences between the approximate and numerical solutions can be seen readily.) The solid line shows the results of numerical calculations, while the long dash line shows the two-term outer solution, and the dotted lines show the one-term inner solutions. The agreement is very reasonable and becomes better for smaller values of ε, as shown in Figure 3 for $\varepsilon = 0.01$. We note that the total twist Tw is numerically found to be $1.4025/(2\pi)$ and $1.3286/(2\pi)$ for the $\varepsilon = 0.05$ and $\varepsilon = 0.01$ cases, respectively, thus confirming our assumption that Tw is $O(1)$.
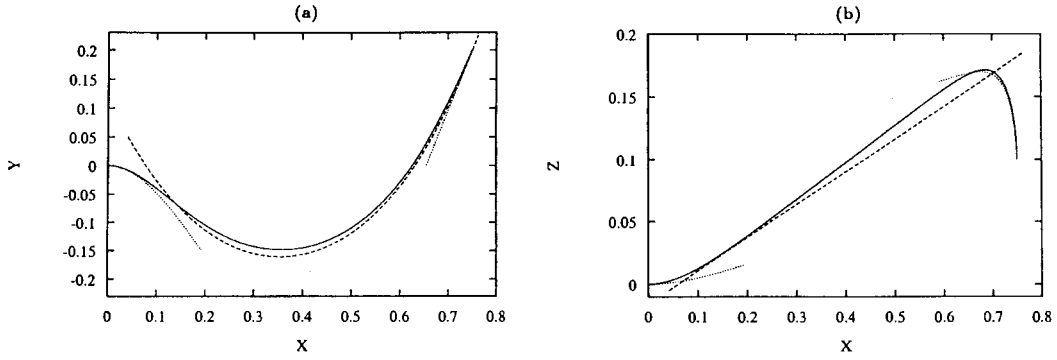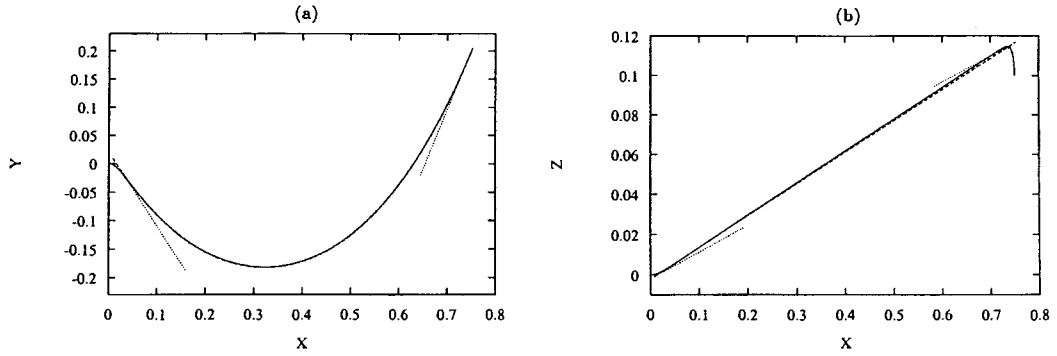
Figure 2. (a) Side view and (b) top view of the outer (dashed), inner (dotted) and numerical (solid) solution of the hanging rod ($a_1 = 0.75$, $a_2 = 0.2$, $a_3 = 0.1$, $\theta_1 = 0°$, $\psi_1 = -90°$, $\phi_1 = 0°$, $\varepsilon = 0.05$, $\kappa = 0.75$).

Figure 3. (a) Side view and (b) top view of the outer (dashed), inner (dotted) and numerical (solid) solution of the hanging rod ($a_1 = 0.75$, $a_2 = 0.2$, $a_3 = 0.1$, $\theta_1 = 0°$, $\psi_1 = -90°$, $\phi_1 = 0°$, $\varepsilon = 0.01$, $\kappa = 0.75$).

In applying the analysis to the laying of a clamped pipeline, it is natural to assume an initial near-catenary shape for the pipeline (a true catenary is not attainable as long as ε is non-zero), which is the situation within the industrial context. The number of independent boundary-value parameters is then reduced by two. In order to see this recall that the *dimensional* catenary in the $(\mathbf{i}, \mathbf{j})$ plane, with rectangular co-ordinates (X, Y), has the form (see, *e.g.*, Meriam and Kraige [19, pp. 305–307])

$$Y = \frac{T_0}{mg}\left(\cosh\frac{mgX}{T_0} - 1\right),$$

$$\theta(s) = \arctan\frac{mgs}{T_0}, \tag{47}$$

$$L^2 = \left(\frac{T_0}{mg} + D\right)^2 - \frac{T_0^2}{m^2 g^2},$$

where: T_0 is the horizontal component of the tension at the top of the catenary, and D is the water depth. The various quantities in Equation (47) are evaluated at the end point $s = L$ and equated with the various boundary conditions, which gives the dimensionless equations

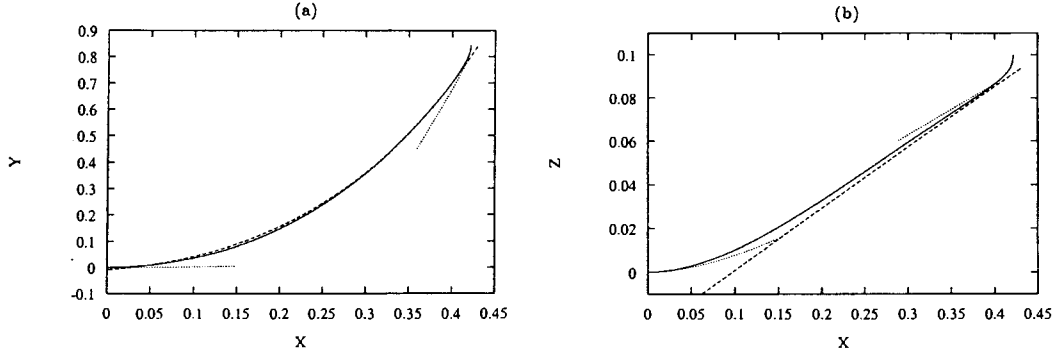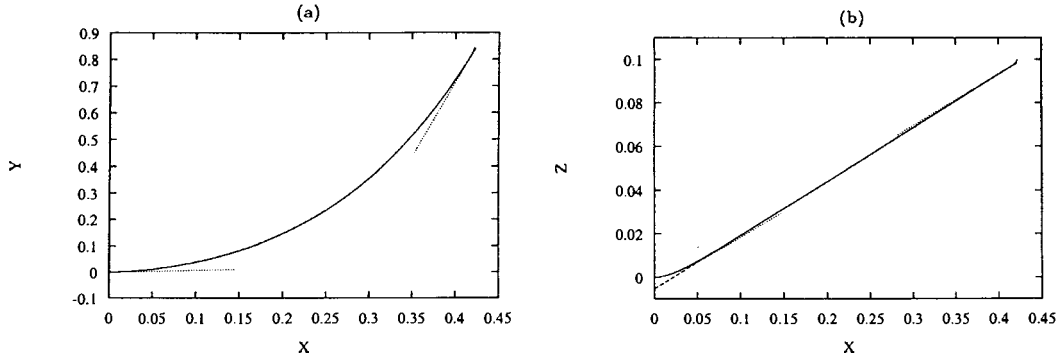$$a_2 = \beta\left(\cosh\frac{a_1}{\beta} - 1\right),$$

Figure 4. Near-catenary solutions: (a) side view and (b) top view of the outer (dashed), inner (dotted) and numerical (solid) solution of the hanging rod ($a_2 = 2a_1$, $a_3 = 0\cdot1$, $\psi_1 = 90°$, $\phi_1 = 0°$, $\varepsilon = 0\cdot05$, $\kappa = 0\cdot75$).

Figure 5. Near-catenary solutions: (a) side view and (b) top view of the outer (dashed), inner (dotted) and numerical (solid) solution of the hanging rod ($a_2 = 2a_1$, $a_3 = 0\cdot1$, $\psi_1 = 90°$, $\phi_1 = 0°$, $\varepsilon = 0\cdot01$, $\kappa = 0\cdot75$).

$$\theta_1 = \arctan \frac{1}{\beta}, \tag{48}$$

$$(a_2 + \beta)^2 = 1 + \beta^2,$$

where β is the dimensionless end tension given by

$$\beta = \frac{T_0}{mgL}. \tag{49}$$

It follows that by specifying one of the quantities a_1, a_2 or θ_1 (or any relationship among them), all three (and β) are fixed.

Figures 4 and 5 show near-catenary solutions satisfying $a_2 = 2a_1$ (giving $\theta_1 = 80\cdot30°$, $a_1 = 0\cdot421760$, $a_2 = 0\cdot843519$, $\beta = 0\cdot170995$), $a_3 = 0\cdot1$ and $\psi_1 = 90°$, for $\varepsilon = 0\cdot05$ and $\varepsilon = 0\cdot01$. Again, the results of the numerical calculations are shown by solid lines, while the long-dash line shows the two-term outer solution and the dotted lines show the one-term inner solutions. The agreement becomes excellent for the smaller value $\varepsilon = 0\cdot01$.

5. Concluding remarks

The method of matched asymptotic expansions has been used to solve the general problem of a clamped bent and twisted three-dimensional rod hanging under gravity and buoyancy
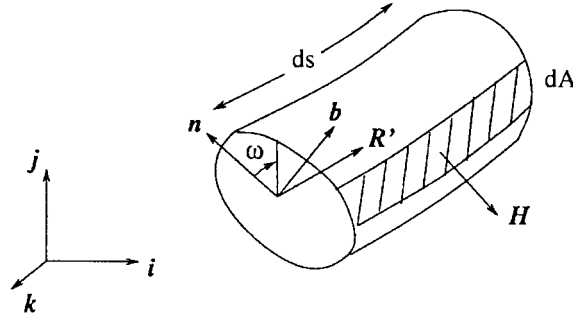
Figure 6. The rod element used for calculating the buoyancy force.

forces. Both fixed twisting moment and fixed rotation boundary conditions are considered. The leading-order term of the inner expansion and the first two terms of the outer expansion are obtained in closed form. To this level of approximation twist does not play a role. The analytical formulation gives good agreement with numerical solutions of the full system of equations. The analysis is also applied to the near-catenary shapes that occur for the laying of a clamped heavy cable or a pipeline.

6. Appendix A: The buoyancy force

The buoyancy force acting on an element of the three-dimensional rod is derived from a modification of Pedersen's analysis [15]. Figure 6 shows a rod element of length ds in a fluid that exerts pressures on the lateral sides. To be consistent with Figure 1, gravity points in the $-j$ direction. The Frenet basis system $\{R', n = R''/|R''|, b = R' \times n\}$ is shown on the lower cross-sectional face of the element, and the angular co-ordinate ω measures the inclination of points along the lateral surface of the rod from the normal direction n (positive ω is inclined towards the binormal b). For clarity, the length of the element ds has been exaggerated relative to the rod radius a. Within the fluid, the pressure distribution is given by

$$p = -\rho_f g(D - y), \tag{A1}$$

where: y is the vertical co-ordinate of a point in the fluid, and ρ_f is the fluid density.

In order to calculate the buoyancy force, the pressure distribution must be integrated over the lateral sides of the element. Since the rod element is bent with a radius of curvature $1/|R''|$, the infinitesimal surface area on the compressive side of the element is slightly smaller than that on the tensile side. The surface area of the small shaded region in Figure 6 is given by

$$dA = a[1 - a|R''|\cos\omega]\,d\omega\,ds$$

and the outward normal to the element is

$$H = n\cos\omega + b\sin\omega.$$

The total buoyancy force acting on the rod element is obtained by evaluating the integral

$$F\,ds = \int p\,H\,dA, \tag{A2}$$

which must be carried out using the y co-ordinates of the points on the lateral face of the rod element (as described by ω in Figure 6) in Equation (A1). It is straightforward to show that the y co-ordinate around the lateral perimeter of the rod element can be written

$$y = \boldsymbol{R} \cdot \boldsymbol{j} + a(\boldsymbol{n} \cdot \boldsymbol{j}) \cos \omega + a(\boldsymbol{b} \cdot \boldsymbol{j}) \sin \omega,$$

where the vertical co-ordinate of the centre line of the rod element is given by $Y = \boldsymbol{R} \cdot \boldsymbol{j}$. The substitution of the various terms in (A2) provides the formula

$$
\begin{aligned}
\boldsymbol{F} = {} & -\rho_f g a \int_0^{2\pi} (D - \boldsymbol{R} \cdot \boldsymbol{j} - a(\boldsymbol{n} \cdot \boldsymbol{j}) \cos \omega - a(\boldsymbol{b} \cdot \boldsymbol{j}) \sin \omega) \\
& (\boldsymbol{n} \cos \omega + \boldsymbol{b} \sin \omega)(1 - a|\boldsymbol{R}''| \cos \omega) \, \mathrm{d}\omega ,
\end{aligned}
\tag{A3}
$$

which, after evaluation of the integral and the introduction of $m_f = \rho_f \pi a^2$ yields

$$\boldsymbol{F} = m_f g[(\boldsymbol{n} \cdot \boldsymbol{j})\boldsymbol{n} + (\boldsymbol{b} \cdot \boldsymbol{j})\boldsymbol{b} + (D - \boldsymbol{R} \cdot \boldsymbol{j})\boldsymbol{R}''] . \tag{A4}$$

Equation (3) is obtained by using the vector identity

$$\boldsymbol{j} = (\boldsymbol{n} \cdot \boldsymbol{j})\boldsymbol{n} + (\boldsymbol{b} \cdot \boldsymbol{j})\boldsymbol{b} + (\boldsymbol{R}' \cdot \boldsymbol{j})\boldsymbol{R}'$$

in Equation (A4).

7. Appendix B: The twist formulation

In order to apply displacement-controlled boundary conditions, a local frame of so-called directors $\{\boldsymbol{d}_1, \boldsymbol{d}_2, \boldsymbol{d}_3\}$ is introduced at each point along the rod. The director $\boldsymbol{d}_3$ points along the rod tangent, that is, $\boldsymbol{d}_3 = \boldsymbol{R}'$, while $\boldsymbol{d}_1$ and $\boldsymbol{d}_2$ form an arbitrarily oriented set of mutually orthogonal vectors in the cross-section of the rod. The Euler angles θ, ψ, ϕ relate the local director frame to the fixed frame $\{\boldsymbol{i}, \boldsymbol{j}, \boldsymbol{k}\}$ as follows:

$$
\begin{aligned}
\boldsymbol{d}_1 = {} & (-\sin \psi \cos \phi + \cos \psi \sin \phi \sin \theta) \, \boldsymbol{i} - \sin \phi \cos \theta \, \boldsymbol{j} \\
& + (\cos \psi \cos \phi + \sin \psi \sin \phi \sin \theta) \, \boldsymbol{k}, \\
\boldsymbol{d}_2 = {} & (\sin \psi \sin \phi + \cos \psi \cos \phi \sin \theta) \, \boldsymbol{i} - \cos \phi \cos \theta \, \boldsymbol{j} \\
& + (-\cos \psi \sin \phi + \sin \psi \cos \phi \sin \theta) \, \boldsymbol{k}, \\
\boldsymbol{d}_3 = {} & \cos \psi \cos \theta \, \boldsymbol{i} + \sin \theta \, \boldsymbol{j} + \sin \psi \cos \theta \, \boldsymbol{k}.
\end{aligned}
\tag{B1}
$$

Note that the two angles θ and ψ completely determine the orientation of the tangent vector $\boldsymbol{d}_3$ and, after an integration, the centreline of the rod. The third angle ϕ is required to specify the orientation of the other two directors $(\boldsymbol{d}_1, \boldsymbol{d}_2)$. A fully rigid loading condition is obtained by specification of the three Euler angles at both ends of the rod.

The parametrisation of Equation (B1) in terms of Euler angles is such that it respects the actual application of the three angles in practice. Specifically, if the transformation matrix in Equation (B1) is denoted by R, then we have the decomposition

$$R = R_\phi R_\psi R_\theta , \tag{B2}$$

where R_θ represents a counterclockwise rotation about k through an angle θ, R_ψ represents a clockwise rotation about j through an angle ψ, and R_ϕ represents a counterclockwise rotation about d_3 through an angle ϕ (see Figure 1). By the nature of the problem, at the top end of the clamped rod only the first two angles will normally be imposed so that the ϕ angle is zero. We now derive an equation for ϕ which imposes the zero-angle boundary condition.

We start by noting that the rate of change of the director frame can be written

$$d_i' = u \times d_i \qquad (i = 1, 2, 3), \tag{B3}$$

where $u = R' \times R'' = \kappa_1 d_1 + \kappa_2 d_2 + \kappa_3 d_3$ is the curvature vector expressed in terms of the director basis at a rod location. The use of Equation (B1) in Equation (B3) provides the relations

$$\begin{aligned}
\theta' &= \kappa_1 \cos\phi - \kappa_2 \sin\phi, \\
\psi' &= (\kappa_1 \sin\phi + \kappa_2 \cos\phi) / \cos\theta, \\
\phi' &= \kappa_3 + \tan\theta \, (\kappa_1 \sin\phi + \kappa_2 \cos\phi),
\end{aligned} \tag{B4}$$

for the rates of change of the Euler angles. The information contained in Equations (B4)$_1$ and (B4)$_2$ is effectively already contained in Equation (1), so we need to be concerned only with the equation for ϕ. Now note that

$$\begin{aligned}
\kappa_1 &= u \cdot d_1 = (R' \times R'') \cdot d_1 = -R'' \cdot d_2, \\
\kappa_2 &= u \cdot d_2 = (R' \times R'') \cdot d_2 = R'' \cdot d_1,
\end{aligned} \tag{B5}$$

and that $\kappa_3 = N'$. Equations (B1) and (B5) then allow Equation (B4)$_3$ to be rewritten as

$$\phi' = N' + \tan\theta \left[(R'' \cdot k) \cos\psi - (R'' \cdot i) \sin\psi \right]. \tag{B6}$$

The use of Equation (B1)$_3$ yields the expressions

$$\begin{aligned}
\sin\theta &= R' \cdot j, \qquad \sin\psi = \frac{R' \cdot k}{\sqrt{1 - (R' \cdot j)^2}}, \\
\cos\theta &= \sqrt{1 - (R' \cdot j)^2}, \qquad \cos\psi = \frac{R' \cdot i}{\sqrt{1 - (R' \cdot j)^2}},
\end{aligned} \tag{B7}$$

which allows the right-hand side of Equation (B6) to be expressed in terms of Cartesian system variables as

$$\phi' = N' - \frac{R' \cdot j}{1 - (R' \cdot j)^2} \left(R' \times R'' \right) \cdot j. \tag{B8}$$

Integration along the length of the rod gives

$$\phi_1 = N'L - \int_0^L \frac{\boldsymbol{R}' \cdot \boldsymbol{j}}{1 - (\boldsymbol{R}' \cdot \boldsymbol{j})^2} \left(\boldsymbol{R}' \times \boldsymbol{R}''\right) \cdot \boldsymbol{j} \, \mathrm{d}s, \tag{B9}$$

where $\phi_1 = \phi(L)$ is the twist angle imposed at the top end of the rod, and the origin of the angle ϕ has been chosen such that $\phi(0) = 0$ (this fixes a direction for $\boldsymbol{d}_1$, and hence $\boldsymbol{d}_2$, in the rod's cross-section). Note that $(\boldsymbol{R}' \times \boldsymbol{R}'') \cdot \boldsymbol{j}$ is the curvature of the rod about $\boldsymbol{j}$, so for a rod deforming in the $(\boldsymbol{i}, \boldsymbol{j})$ plane, the accrued angle ϕ_1 along the entire length of the rod equals the total twist. It is important to note that the above analysis assumes that θ does not go through $\pi/2$, at which angle a singularity occurs. For a heavy cable or pipeline hanging under gravity, this assumption is normally satisfied.

Nomenclature

s, L	arclength co-ordinate, rod length;	$\boldsymbol{i}, \boldsymbol{j}, \boldsymbol{k}$	Cartesian basis vectors;
θ, ψ, ϕ	Euler angles;	D	depth of immersion fluid;
X, Y, Z	Cartesian components of the position vector;	$\boldsymbol{R}(s), \boldsymbol{R}'(s)$	position and tangent vectors;
T, Q	tangential tension and twisting moment;	$\boldsymbol{V}, \boldsymbol{M}$	shear force and bending moment vectors;
m, g	rod mass density per arclength and gravitational acceleration;	$\boldsymbol{F}$	the buoyancy force per arclength;
N', Tw	the rate of material rotation and the total twist along the rod;	B, K	bending and torsional rigidities;
E, G, ν	Young's modulus, shear modulus, and Poisson's ratio;	I, J	the second area moment and polar moment of inertia;
$\boldsymbol{n}, \boldsymbol{b}$	principal normal and binormal vectors;	m_f, σ	the linear mass density of displaced fluid, the ratio of mass densities m_f/m;
$\boldsymbol{A}_0, \boldsymbol{A}_1$	position boundary conditions;	$\boldsymbol{B}_0, \boldsymbol{B}_1$	tangent boundary conditions;
ε, κ	the dimensionless bending rigidity and the ratio of torsional rigidity to bending rigidity;	$\boldsymbol{C}, \boldsymbol{C}_n$	constant force vector and components on $O(\varepsilon^n)$;
$\boldsymbol{R}_n(s)$	$O(\varepsilon^n)$ position vector in the outer layer;	x_0, y_0, z_0	components of $\boldsymbol{R}_0$;
c_x, c_y, c_z	components of $\boldsymbol{C}_0$;	α	signum(c_x);
X_0, Y_0, Z_0	integration constants for $\boldsymbol{R}_0(s)$;	χ	angle between catenary plane and the x-axis;
x_1, y_1, z_1	components of $\boldsymbol{R}_1$;	d_x, d_y, d_z	components of $\boldsymbol{C}_1$;
X_1, Y_1, Z_1	integration constants for $\boldsymbol{R}_1(s)$;	$\xi, \hat{\boldsymbol{R}}(\xi)$	scaled co-ordinate and position vector for boundary layer near $s = 0$;
$\hat{\boldsymbol{R}}_n(\xi)$	$O(\varepsilon^n)$ position vector in the inner layer;	$\boldsymbol{e}_\rho, \boldsymbol{e}_\eta, N$	local basis vectors at $s = 0$;
$\rho(\xi), h(\xi)$	components of $\hat{\boldsymbol{R}}_0(\xi)$;	$D_0, r_0, \rho_\infty, h_0$	integration constants for $\hat{\boldsymbol{R}}_0(\xi)$;
r	rescaled boundary layer co-ordinate;	$\zeta, \check{\boldsymbol{R}}(\zeta)$	scaled co-ordinate and position vector for the boundary layer near $s = L$;
$\check{\boldsymbol{R}}_n(\zeta)$	$O(\varepsilon^n)$ position vector in the inner layer;	$\boldsymbol{e}_\gamma, \boldsymbol{e}_\sigma, P$	local basis vectors at $s = L$;
r_1, σ_∞, h_1	integration constants for $\check{\boldsymbol{R}}_0(\zeta)$;	$\eta(\varepsilon), \tau$	intermediate co-ordinates for matching the layers;

a_1, a_2, a_3	components of the dimensionless $\boldsymbol{A}_1$;	β, T_0	parameters for near-catenary solutions;
ω, a	angle between normal and binormal vectors, rod radius;	p, ρ_f, y	fluid pressure, volume density of the fluid, vertical co-ordinate in the fluid;
$\boldsymbol{H}, \mathrm{d}A$	outward lateral normal and infinitesimal surface area of rod element;	$\boldsymbol{d}_1, \boldsymbol{d}_2, \boldsymbol{d}_3$	material director basis;
$\boldsymbol{u}$	the curvature vector;	$\kappa_1, \kappa_2, \kappa_3$	components of the curvature vector in the director basis.

Acknowledgements

References

1. M. J. Brown and L. Elliott, Pipelaying from a barge. *Math. Engng. Ind.* 1 (1987) 33–46.
2. A. H. Nayfeh, *Perturbation Methods*. New York: John Wiley & Sons (1973) 425 pp.
3. J. Kevorkian and J. D. Cole, *Multiple Scale and Singular Perturbation Methods*. Berlin: Springer-Verlag (1996) 632 pp.
4. R. Plunkett, Static bending stresses in catenaries and drill strings. *Trans. ASME J. Eng. for Industry* 89 (1967) 31–36.
5. S. W. Rienstra, Analytical approximations for offshore pipeline problems. In: A.H.P. van der Burgh and R.M.M. Mattheij (eds.), *Proceedings of the First International Conference on Industrial and Applied Mathematics ICIAM 87 (contributions from the Netherlands)*. Amsterdam: CWI Tracts (1987) 99–108.
6. D. A. Dixon and D. R. Rutledge, Stiffened catenary calculations in pipeline laying problem. *Trans. ASME J. Eng. for Industry* 90 (1968) 153–160.
7. I. Konuk, Higher order approximations in stress analysis of submarine pipelines. *Trans. ASME J. Energy Res. Technology* 102 (1980) 190–196.
8. P. Wolfe, The effect of bending stiffness on inextensible cable. *Int. J. Engng. Sci.* 30 (1992) 1187–1192.
9. P. Wolfe, Hanging cables with small bending stiffness. *Nonlinear Anal. T.M.A.* 20 (1993) 1193–1204.
10. I. Konuk, Application of an adaptive numerical technique to 3-D pipeline problems with strong nonlinearities, *Trans. ASME J. Energy Res. Technology* 104 (1982) 58–62.
11. D. M. Stump and W. B. Fraser, Bending boundary layers in a moving strip. *Nonlinear Dynamics* (in press).
12. A. E. H. Love, *A Treatise on the Mathematical Theory of Elasticity*. 4th ed. Cambridge: Cambridge University Press (1927) 643 pp.
13. S. S. Antman, *Nonlinear Problems of Elasticity* Berlin: Springer-Verlag (1995) 750 pp.
14. A. R. Champneys, G. H. M. van der Heijden and J. M. T. Thompson, Spatially complex localization after one-twist-per-wave equilibria in twisted circular rods with initial curvature. *Phil. Trans. R. Soc. Lond.* A 355 (1997) 2151–2174.
15. P. T. Pedersen, Equilibrium of offshore cables and pipelines during laying. *Int. Shipbuilding Progress* 22 (1975) 399–408.
16. J. Coyne, Analysis of the formation and elimination of loops in twisted cable. *IEEE J. Ocean. Eng.* 15 (1990) 72–83.
17. M. Van Dyke, *Perturbation Methods in Fluid Mechanics*, Stanford: Parabolic Press (1975) 271 pp.
18. U. Ascher, J. Christiansen and R. D. Russell, Collocation software for boundary-value ODEs. *ACM Trans. Math. Software* 7 (1981) 209–222. The COLNEW code is freely available at http://www.netlib.org/ode/.
19. J. L. Meriam and L. G. Kraige, *Engineering Mechanics, Volume 1: Statics, Third Edition*. New York: John Wiley & Sons (1992) 533 pp.